Available online at www.sciencedirect.com
SCIENCE DIRECT®
Polyhedron 25 (2006) 1864–1872
POLYHEDRON
www.elsevier.com/locate/poly

Metal complexes of 21-(4-*tert*-butyl-benzenesulfonamido)-5,10,15,20-tetraphenyl-porphyrin: Ga(*N*-*p*-$NSO_2C_6H_4{}^tBu$-tpp)(OH), Tl(*N*-*p*-$NSO_2C_6H_4{}^tBu$-tpp)(O_2CCF_3) and Zn(*N*-*p*-$NSO_2C_6H_4{}^tBu$-tpp) [tpp = 5,10,15,20-tetraphenylporphyrinate]

Wei-Zhi Shil [a], Kuan-Yu Cho [a], Ching-Wen Cheng [a], Jyh-Horung Chen [a,*], Shin-Shin Wang [b,*], Feng-Ling Liao [c], Jo-Yu Tung [d], Hsi-Ying Hsieh [d], Shanmugam Elango [e]

[a] *Department of Chemistry, National Chung-Hsing University, Taichung 40227, Taiwan*
[b] *Union Chemical Laboratories, Hsin-Chu 300, Taiwan*
[c] *Department of Chemistry, National Tsing-Hua University, Hsin-Chu 300, Taiwan*
[d] *Chung Hwa College of Medical Technology, Tainan 717, Taiwan*
[e] *Institute of Chemical and Engineering Sciences, Singapore 627833, Singapore*

Received 20 September 2005; accepted 7 December 2005
Available online 20 January 2006

Abstract

The crystal structures of *trans*-hydroxo-*N*-*p*-*tert*-butylbenzenesulfonylimido-*meso*-tetraphenylporphyrinatogallium(III) 0.5 aqua and 0.5 methanol solvate [Ga(*N*-*p*-$NSO_2C_6H_4{}^tBu$-tpp)(OH) · 0.5MeOH · 0.5H_2O; **2** · 0.5MeOH · 0.5H_2O], *cis*-trifluoroacetato-*N*-*p*-*tert*-butylbenzenesulfonylimido-*meso*-tetraphenylporphyrinatothallium(III) [Tl(*N*-*p*-$NSO_2C_6H_4{}^tBu$-tpp)(O_2CCF_3); **3**] and *N*-*p*-*tert*-butylbenzenesulfonylimido-*meso*-tetraphenylporphyrinatozinc(II) 0.7 methanol solvate [Zn(*N*-*p*-$NSO_2C_6H_4{}^tBu$-tpp) · 0.7MeOH; **4** · 0.7MeOH], were determined. The coordination sphere around Tl^{3+} ion in **3** is a distorted square-based pyramid in which the apical site is occupied by a chelating bidentate $CF_3CO_2^-$ group, whereas for the Ga^{3+} ion in **2**, it is a distorted trigonal bipyramid with N(2), N(4), and O(1) lying in the equatorial plane. The geometry around Zn^{2+} in **4** is a distorted square planar. The free energy of activation at the coalescence temperature T_c for the intermolecular trifluoroacetate exchange process for **3** in CD_2Cl_2 is found to be $\Delta G^{\ddagger}_{223} = 46.3$ kJ/mol through ^{19}F NMR variable temperature measurements.

In the slow-exchange region, the CF_3 and carbonyl (CO) carbons of the $CF_3CO_2^-$group of **3** in CD_2Cl_2 are separately located at δ 115.9 [^3J(Tl–^{13}C) = 155 Hz] and 160.2 [^2J(Tl–^{13}C) = 81 Hz] at −90 °C.

Keywords: Thallium; X-ray diffraction; Gallium; Dynamic NMR; TFA ligands

1. Introduction

Metalloporphyrins with a bridged structure between the central metal and one of the four pyrrole nitrogens have drawn much attention in recent times bridged metalloporphyrins with M–NX–N linkages [X = Ts = tosyl, *p*-$COC_6H_4NO_2$ (*p*-nitrobenzoyl), or COC_6H_5 (benzamido)] have so far been reported [1–7]. Upon replacement of CH_3 of tosyl by a bulkier and heavier ^tBu group, the free base *N*-*p*-$HNSO_2C_6H_4CH_3$-Htpp (tpp = dianion of *meso*-tetraphenylporphyrin) became 21-(4-*tert*-butyl-benzenesulfonamido)-5,10,15,20-tetraphenyl-porphyrin *N*-*p*-$HNSO_2$-$C_6H_4{}^tBu$-Htpp (**1**). The d^{10} configuration permits a wide variety of geometries and coordination numbers. However

* Corresponding authors.
E-mail address: jyhhchen@dragon.nchu.edu.tw (J.-H. Chen).

0277-5387/$ - see front matter © 2005 Elsevier Ltd. All rights reserved.
doi:10.1016/j.poly.2005.12.006

there were no X-ray structural data available for the metal ion [M(II) and M(III)] complexes of *N-p*-$HNSO_2C_6H_4{}^tBu$-Htpp (**1**). The effect of coordination of a variety of d^{10} metals namely zinc(II), gallinum(III) and thallium(III) on pophyrin macrocycles is of great interest, because the structural analysis of these metal complexes could be expected to discover the effects due to the incorporation of d^{10} metal ions (i.e., Zn^{2+}, Ga^{3+} and Tl^{3+}) into the highly distorted and relatively rigid coordination environment provided by the aminated porphyrin ligand **1**. The bulky ^{t}Bu group in this system enhances the crystallization of metal these complexes.

In this paper, we described the synthesis and X-ray structural investigation on the metallation of **1** leading to mononuclear complexes of *trans*-hydroxo-*N-p-tert*-butylbenzenesulfonylimido-*meso*-tetraphenylporphyrinatogallium(III) 0.5 aqua and 0.5 methanol solvate [Ga(*N-p*-$NSO_2C_6H_4{}^tBu$-tpp)(OH) · 0.5MeOH · 0.5H_2O; **2** · 0.5MeOH · 0.5H_2O], *cis*-trifluoroacetato-*N-p-tert*-butylbenzenesulfonylimido-*meso*-tetraphenylporphyrinatothallium(III) [Tl(*N-p*-$NSOC_6H_4{}^tBu$-tpp)(O_2CCF_3); **3**] and *N-p-tert*-butylbenzenesulfonylimido-*meso*-tetraphenylporphyrinatozinc(II) 0.7 methanol solvate [Zn(*N-p*-$NSO_2C_6H_4{}^tBu$-tpp) · 0.7MeOH; **4** · 0.7MeOH]. It is observed that the ionic radius increases from 0.69 Å for Ga^{3+} to 0.74 Å for Zn^{2+} and to 1.025 Å for Tl^{3+} [8]. Furthermore, we tried to figure out the relative positions of the $CF_3CO_2^-$ (or OH^-) and *N*-^{t}BuBS (^{t}BuBS = 4-*tert*-butylbenzenesulfonyl = SO_2C_6- $H_4{}^tBu$) groups coordinated to the metal atom lead to a *cis* configuration in **3** and a *trans* configuration in **2** that might depend on the ionic radius of the Tl^{3+} and Ga^{3+}. In addition, the trifluoroacetato (TFA) exchange of Tl(tpp)(O_2CCF_3) observed in THF-d_8 prompted us to investigate a similar intermolecular exchange for complex **3** in CD_2Cl_2 by ^{19}F and ^{13}C dynamic NMR methods [9].

2. Experimental

2.1. N-p-$HNSO_2C_6H_4{}^tBu$-Htpp (1)

A mixture of NaN_3 (1 g, 1.54×10^{-2} mol) in distilled water (2 cm^3) and *N*-4-*tert*-butylbenzenesulfonyl chloride (1 g, 4.31×10^{-3} mol) in acetone (20 cm^3) was stirred for 1 h. After concentration, the residue was taken in CH_2Cl_2 and collected by filtration to remove the excess of NaN_3. The CH_2Cl_2 layer contains *p*-^{t}Bu-C_6H_4-SO_2N_3. A solution of Zn(tpp) (0.27 g, 3.04×10^{-4} mol) and the above ^{t}Bu-C_6H_4-SO_2N_3 in CH_2Cl_2 (200 cm^3) in a stoppered 250 mL Erlenmeyer flask was left for ca. 8 h in the sunlight. After that to this solution was added 0.5 N HCl (250 cm^3) with vigorous shaking for 0.5 h. The organic layer was separated, solid ammonium carbonate was added to it, and then dried with anhydrous Na_2SO_4. The excess $(NH_4)_2CO_3$ and Na_2SO_4 were removed by filtration. After concentration, the residue was dissolved in a minimum of CH_2Cl_2 and chromatographed on silica gel (100 g, 70–230 mesh). The desired compound was eluted with ethyl acetate–CH_2Cl_2 [1:2 (v/v)] as dark brown band on silica gel. Removal of the solvent and recrystallization from CH_2Cl_2–MeOH [1:3 (v/v)] gave the bluish-purple solid of **1** (0.17 g, 2.06×10^{-4} mol, 68%). ^1H NMR (599.95 MHz, $CDCl_3$, 20 °C): δ 8.97 [d, H_β, ^3J(H–H) = 5 Hz]; 8.93 [d, H_β, ^3J(H–H) = 5 Hz]; 8.81 (s, H_β); 8.46 [d, ^3J(H–H) = 7 Hz] and 8.10 [d, ^3J(H–H) = 8 Hz] for *ortho* protons; 7.91(s, H_β); 7.87–7.81 (m) and 7.78–7.73 (m) for *meta* and *para* protons; 6.65 [d, ^{t}BuBS-$H_{3,5}$, ^3J(H–H) = 8 Hz], where ^{t}BuBS = 4-*tert*-butylbenzenesulfonyl; 4.94 [d, ^{t}BuBS-$H_{2,6}$, ^3J(H–H) = 8 Hz]; 1.13 (s, *t*-butyl protons); 0 (s, NH). FAB-MS, *m/z* (assignment, rel intensity): 826 ([*N-p*-$HNSO_2C_6H_4{}^tBu$-Htpp)]$^+$, 100), 614([(H_2tpp)]$^+$, 93.89). UV/visible spectrum, λ (nm) [$\varepsilon \times 10^{-3}$ (M^{-1} cm^{-1})] in CH_2Cl_2: 320 (24.7), 433 (339), 548 (15.0), 584 (15.9), 638 (13.7).

2.2. Ga(N-p-$NSO_2C_6H_4{}^tBu$-tpp)(OH) (2)

Free base *N-p*-$HNSO_2C_6H_4{}^tBu$-Htpp (**1**) (0.05 g, 6.05×10^{-5} mol) and Ga_2O_3 (0.1 g, 5.34×10^{-4} mol) were refluxed for 12 h in 100 cm^3 of acetic acid containing sodium acetate (0.05 g). After removal of the solvent (HOAc) under reduced pressure, the residue was dissolved in CH_2Cl_2 and then dried over Na_2SO_4. After filtration, the filtrate was rotavaped and recrystallization from CH_2Cl_2/MeOH [1:3 (v/v)] afforded a purple solid of **2** (0.036 g, 3.95×10^{-5} mol, 65%). Compound **2** was dissolved in CH_2Cl_2 and layered with MeOH to get purple crystals of **2** for single crystal X-ray analysis. ^1H NMR (599.95 MHz, $CDCl_3$, 20 °C): δ 9.22 [s, H_β(4,5)], H_β(a,b) represents the two equivalent β-pyrrole protons attached to carbons a and b, respectively; 8.75 [d, H_β(10,19), ^3J(H–H) = 4.8 Hz]; 8.71 [d, H_β(9,20), ^3J(H–H) = 4.8 Hz]; 7.85 [s, H_β(14,15)]; 8.36 [s, *o*′-H(38,40)], *o*′-H represents *ortho* phenyl protons; 8.06 [d, *o*′-H(34,44), ^3J(H–H) = 4.3 Hz]; 8.34 [m, *o*-H(26,28)]; 8.29 [d, *o*-H(22,32), ^3J(H–H) = 5.4 Hz]; 7.74–7.85 (m) for *meta* and *para* protons; 6.58 [d, ^{t}BuBS-$H_{3,5}$, or H(47,49), ^3J(H–H) = 8.4 Hz]; 4.72 [d, ^{t}BuBS-$H_{2,6}$, or H(46,50), ^3J(H–H) = 8.4 Hz]; 1.03 (s, *t*-butyl protons); −1.98 (s, OH). FAB-MS, *m/z* (assignment, rel intensity): 894 ([Ga(*N-p*-$NSO_2C_6H_4{}^tBu$-tpp)]$^+$, 11.19), 892 ([Ga(*N-p*-$NSO_2C_6H_4$-^{t}Bu-tpp) − 2H]$^+$, 11.90), 681 ([Ga(tpp)-H]$^+$, 49.40), 154 ([NBA + H]$^+$, 68.01). UV/visible spectrum, λ (nm) [$\varepsilon \times 10^{-3}$ (M^{-1} cm^{-1})] in CH_2Cl_2: 434 (315), 547 (11.4), 585 (14.6), 634 (4.3).

2.3. Tl(N-p-$NSO_2C_6H_4{}^tBu$-tpp)(O_2CCF_3) (3)

A mixture of Tl(O_2CCF_3)$_3$ (0.07 g, 1.29×10^{-4} mol) in MeOH (10 cm^3) and *N-p*-$HNSO_2C_6H_4{}^tBu$-Htpp (0.05 g, 6.05×10^{-5} mol) in CH_2Cl_2 (20 cm^3) was refluxed in CH_3CN (50 cm^3) for 3 h. After concentrating, the residue was dissolved in CH_2Cl_2, dried with anhydrous Na_2SO_4 and filtered. The filtrate was concentrated and recrystallized from CH_2Cl_2–MeOH [1:5 (v/v)] yielding blue solid of **3** (0.035 g, 3.07×10^{-5}mol, 50.7%) which was again

dissolved in CH_2Cl_2 and layered with MeOH to get blue crystals for single crystal X-ray analysis. ^{1}H NMR (299.96 MHz, CD_2Cl_2, 20 °C): δ 9.16 [d d, H_β(10,19), ^4J(Tl–H) = 17.5 Hz and ^3J(H–H)] = 4.8 Hz; 9.03 [d d, H_β(9,20), ^4J(Tl–H) = 10.3 Hz and ^3J(H–H) = 4.8 Hz]; 8.81 [d, H_β(4,5), ^4J(Tl–H) = 90.0 Hz]; 7.03 [s, H_β(14,15)]; 8.38 [d, *o*-H(26,32), ^3J(H–H) = 5.4 Hz]; 8.15 [d, *o*-H(22, 28), ^3J(H–H) = 6.6 Hz]; 7.80–7.90 (m) for *meta* and *para* protons; 7.13 [d, ^{t}BuBS-$H_{3,5}$, or H(47,49), ^3J(H–H) = 8.0 Hz]; 6.13 [d, ^{t}BuBS-$H_{2,6}$, or H(46,50), ^3J(H–H) = 8.0 Hz]; 1.19 (s, *t*-butyl protons). ^{19}F NMR (564.49 MHz, CD_2Cl_2, 20 °C): δ −73.50 (s). FAB-MS, *m*/*z* (assignment, rel intensity): 1028 ([Tl(*N*-*p*-$NSO_2C_6H_4{}^t$Bu-tpp)]$^+$, 39.58), 826 ([H*N*-*p*-$NSO_2C_6H_4{}^t$Bu-Htpp]$^+$, 54.23), 154 ([NBA+H]$^+$, 100). UV/visible spectrum, λ (nm) [$\varepsilon \times 10^{-3}$ (M^{-1} cm^{-1})] in CH_2Cl_2: 336 (18.2), 447 (259), 556 (6.55), 608 (14.6).

2.4. Zn(N-p-$NSO_2C_6H_4{}^t$Bu-tpp) (4)

Compound **4** was prepared in the same way as described for Tl(*N*-*p*-$NSO_2C_6H_4{}^t$Bu-tpp)(OAc) using $Zn(OAc)_2$ in 80% yield [14]. Compound **4** was dissolved in CH_2Cl_2 and layered with MeOH and purple crystals of **4** · 0.7MeOH were obtained for single crystal X-ray analysis. ^{1}H NMR (599.95 MHz, $CDCl_3$, 20 °C): δ 8.96 [d, H_β(7,18), ^3J(H–H) = 4.2 Hz]; 8.90 [d, H_β(8,17), ^3J(H–H) = 4.8 Hz]; 8.82 [s, H_β(12,13)]; 8.46 [d, *o*-H(32,34), ^3J(H–H) = 7.2 Hz]; 8.10 [d, *o*-H(28,38), ^3J(H–H) = 7.2 Hz]; 8.21 (bs) and 7.89 (bs) for the other set of *ortho* protons (*o*′-H); 7.85 [t, ^3J(H–H) = 7.8 Hz], 7.74 (m) and 7.68 (bs) for *meta* protons; 7.81 [t, *para* H, ^3J(H–H) = 7.8 Hz]; 6.89 [d, ^{t}BuBS-$H_{3,5}$, or H(47,49), ^3J(H–H) = 8 Hz]; 5.58 [d, ^{t}BuBS-$H_{2,6}$, or H(46,50), ^3J(H–H) = 8 Hz]; 1.15 (s, *t*-butyl protons). ESI-MS, *m*/*z* (assignment, rel intensity): 888 ([Zn(*N*-*p*-$NSO_2C_6H_4{}^t$Bu-tpp) + H]$^+$, 22.08), 690 ([Zn(tpp)$^+$N − 2H]$^+$, 100). UV/visible spectrum, λ (nm) [$\varepsilon \times 10^{-3}$ (M^{-1} cm^{-1})] in CH_2Cl_2: 322 (20.5), 437 (299), 557 (9.9), 603 (16.1).

2.5. Spectroscopy

Proton and ^{13}C NMR spectra were recorded at 299.95 (or 599.95) and 75.43 (or 150.87) MHz, respectively, on Varian VXR-300 (or Varian Unity Inova-600) spectrometers locked on deuterated solvent, and referenced to the solvent peak. Proton NMR is relative to CD_2Cl_2 or $CDCl_3$ at δ = 5.30 or 7.24 and ^{13}C NMR to the center line of CD_2Cl_2 or $CDCl_3$ at δ = 53.6 or 77.0. ^{19}F NMR spectra were measured in CD_2Cl_2 at 564.49 MHz in a Varian Unity Inova-600 spectrometer. ^{19}F NMR data are internally referenced to $CFCl_3$. The temperature of the spectrometer probe was calibrated by the shift difference of the methanol resonance in the ^{1}H NMR spectrum. HMQC (heteronuclear multiple quantum coherence) was used to correlate protons and carbon through one-bond coupling and HMBC (heteronuclear multiple bond coherence) for two- and three-bond proton–carbon coupling. nuclear Overhauser effect (NOE) difference spectroscopy was employed to determine the ^{1}H–^{1}H proximity through space over a distance of up to about 4 Å.

Positive ion mode ESI mass spectra were acquired at room temperature on a ThermoFinnigan LCQ Advantage mass spectrometer. The positive-ion fast atom bombard-

Table 1
Crystal data for **2** · 0.5MeOH · 0.5H_2O, **3** and **4** · 0.7MeOH

Empirical formula	$C_{54.50}H_{45}GaN_5O_4S$ (**2** · 0.5MeOH · 0.5H_2O)	$C_{56}H_{41}F_3N_5O_4STl$ (**3**)	$C_{54.70}H_{43.80}N_5O_{2.70}SZn$ (**4** · 0.7MeOH)
Formula weight	935.73	1141.37	911.78
Space group	$P\bar{1}$	$P\bar{1}$	$P2_1/c$
Crystal system	triclinic	triclinic	monoclinic
a (Å)	10.6962(6)	12.2694(7)	14.8830(18)
b (Å)	13.3596(8)	14.4713(8)	12.2593(16)
c (Å)	18.3789(11)	14.5566(8)	25.427(3)
α (°)	72.373(1)	79.540(1)	90
β (°)	87.530(1)	70.512(1)	100.010(2)
γ (°)	67.930(1)	86.048(1)	90
V (Å^3)	2312.1(2)	2395.9(2)	4568.7(10)
Z	2	2	4
F(000)	972	1136	1916
D_{calc} (g cm^{-3})	1.344	1.582	1.338
μ(Mo Kα) (mm^{-1})	0.693	3.480	0.635
S	1.003	1.006	1.082
Crystal size (mm^3)	0.30 × 0.25 × 0.25	0.50 × 0.20 × 0.10	0.68 × 0.32 × 0.18
$2\theta_{max}$ (°)	56.68	56.60	52.16
T (K)	100(2)	100(2)	295(2)
Number of reflections measured	11 429	11 836	9005
Number of reflections observed	8285	10 564 ($I > 2\sigma(I)$)	5133 ($I > 2\sigma(I)$)
R_1[a]	0.0522	0.0292	0.0493
wR_2[b]	0.1476	0.0711	0.1261

[a] $R_1 = [\sum ||F_o| - |F_c|| / \sum |F_o|]$.
[b] $wR_2 = [\sum w(F_o^2 - F_c^2)^2 / \sum w(F_o^2)^2]^{1/2}$.

Table 2
Selected bond lengths (Å) and angles (°) for compounds **2** · 0.5MeOH · 0.5H_2O, **3** and **4** · 0.7MeOH

Ga(*N*-*p*-$NSO_2C_6H_4{}^t$Bu-tpp)(OH) · 0.5MeOH · 0.5H_2O (**2** · 0.5MeOH · 0.5H_2O)			
Bond lengths			
Ga(1)–N(1)	2.305(2)	Ga(1)–N(4)	1.959(2)
Ga(1)–N(2)	1.914(2)	Ga(1)···N(5)	2.638(2)
Ga(1)–N(3)	2.048(2)	Ga(1)–O(1)	1.835(2)
Bond angles			
O(1)–Ga(1)–N(1)	90.40(9)	Ga(1)–N(4)–N(5)	102.95(16)
O(1)–Ga(1)–N(2)	118.66(10)	N(4)–Ga(1)–N(1)	84.38(10)
O(1)–Ga(1)–N(3)	95.65(10)	N(4)–Ga(1)–N(2)	127.18(10)
O(1)–Ga(1)–N(4)	114.13(10)	N(4)–Ga(1)–N(3)	83.33(9)
Ga(1)–N(4)–S(1)	140.11(14)		
Tl(*N*-*p*-$NSO_2C_6H_4{}^t$Bu-tpp)(O_2CCF_3) (**3**)			
Bond lengths			
Tl(1)–O(3)	2.426(2)	Tl (1)–N(2)	2.120(2)
Tl(1)–O(4)	2.427(2)	Tl (1)–N(3)	2.329(2)
Tl(1)–N(1)	2.363(2)	Tl(1)···N(4)	2.880(2)
		Tl (1)–N(5)	2.081(2)
Bond angles			
O(3)–Tl(1)–N(1)	136.05(8)	O(4)–Tl(1)–N(1)	83.83(8)
O(3)–Tl(1)–N(2)	93.64(9)	O(4)–Tl(1)–N(2)	102.20(9)
O(3)–Tl(1)–N(3)	103.77(9)	O(4)–Tl(1)–N(3)	157.44(9)
O(3)–Tl(1)–N(5)	110.86(9)	O(4)–Tl(1)–N(5)	97.07(8)
O(3)–Tl(1)–O(4)	54.30(8)	Tl(1)–N(5)–N(4)	110.84(17)
Zn(*N*-*p*-$NSO_2C_6H_4{}^t$Bu-tpp) · 0.7MeOH (**4** · 0.7MeOH)			
Bond lengths			
Zn–N(2)	2.074(3)	Zn–N(5)	1.983(3)
Zn–N(3)	1.943(3)	Zn–O(3)	2.342(6)
Zn–N(4)	2.060(3)	Zn···N(1)	2.627(6)
Bond angles			
N(5)–Zn–N(2)	90.08(11)	Zn–N(5)–N(1)	100.50(18)
N(5)–Zn–N(3)	171.74(11)	Zn–N(5)–S	144.29(16)
N(5)–Zn–N(4)	88.70(11)		

ment mass spectrum (FAB MS) was obtained in a nitrobenzyl alcohol (NBA) matrix using a JEOL JMS-SX/SX 102A mass spectrometer. UV/visible spectra were recorded at 20 °C on a HITACHI U-3210 spectrophotometer.

2.6. Crystallography

Table 1 presents the crystal data as well as other information for **2** · 0.5MeOH · 0.5H_2O, **3**, and **4** · 0.7MeOH. Measurements were taken on a Bruker AXS SMART-1000 diffractometer using monochromatized Mo Kα radiation ($\lambda = 0.71073$ Å). Empirical absorption corrections were made for **2** · 0.5MeOH · 0.5H_2O and **3**. The SADABS absorption corrections were made for **4** · 0.7MeOH. The structures were solved by direct methods (SHELXTL PLUS) and refined by the full-matrix least-squares method. All non-hydrogen atoms were refined with anisotropic thermal parameters, whereas all hydrogen atoms were placed in calculated positions and refined with a riding model. Table 2 lists selected bond distances and angles for these three complexes.

3. Results and discussion

3.1. Molecular structures of 2 · 0.5MeOH · 0.5H_2O, 3 and 4 · 0.7MeOH

The X-ray structures are depicted in Fig. 1a for the complex Ga(*N*-*p*-$NSO_2C_6H_4{}^t$Bu-tpp)(OH) · 0.5MeOH · 0.5H_2O (or **2** · 0.5MeOH · 0.5H_2O), in Fig. 1b for Tl-(*N*-*p*-$NSO_2C_6H_4{}^t$Bu-tpp)(O_2CCF_3) **3** and in Fig. 1c for Zn-(*N*-*p*-$NSO_2C_6H_4{}^t$Bu-tpp) · 0.7MeOH (**4** · 0.7MeOH). Their structures are a five-coordinate gallium, a six-coordinate thallium, and a four-coordinate zinc, having three nitrogen atoms of the porphyrins and one extra nitrogen atom of the $NSO_2C_6H_4{}^t$Bu fragment in common, but they are different with one more chelating bidentate $CF_3CO_2^-$ ligand for **3** in the axial site and one more axial OH^- ligand for **2**. The metal–ligand bond distances, i.e., from Ga(III), Tl(III), and Zn(II) atoms to the ligand and the angles are summarized in Table 2. The bond distances are Ga(1)–O(1) = 1.835(2) Å and the mean Ga(1)–N(p) = 1.969(2) Å for **2** · 0.5MeOH · 0.5H_2O; for **3**, the similar values are Tl(1)–O(3) = 2.426(2) Å, Tl(1)–O(4) = 2.427(2) Å and the mean Tl(1)–N(p) = 2.223(2) Å. The interaction of the trifluoroacetate with thallium is chelating bidentate. This kind of bidentate interaction was previously observed for Tl(tpp)(O_2CCF_3) with Tl–O(1) = 2.309(7) Å and Tl–O(2) = 2.64(1) Å [9]. Hence, the geometry around Tl is a distorted square-base pyramid in which the apical site is occupied by a chelating bidentate $CF_3CO_2^-$ group. The bond distance (Å) of Zn–O(3) is 2.342(6) Å and the mean Zn–N(p) = 2.015(3) Å for **4** · 0.7MeOH. The Zn–O(3)-(MeOH) distance of 2.342(6) Å is longer than the sum of the covalent radii of Zn and O (1.93 Å) but is shorter than the sum of the Van der Waals radii of Zn and O (2.90 Å) [8]. This longer Zn···O(3) contact is too long to be considered as a true coordinated bond and may be viewed as a secondary intermolecular interaction. Hence, the geometry around Zn^{2+} is a distorted square planar in **4**. The observed H(3)···O(1) and O(1)···O(3) distances were 2.16 and 2.69 Å, respectively. These distances fall below those expected from Van der Waals distances of 2.60 and 2.80 Å, respectively. The O(1)–H(3)–O(3) angle was 158.5° and its deviation from linearity was not too severe. Therefore, a hydrogen bond exists between H(3) and the O(1) atom in **4**.

The distortion in five-coordinate complexes can be quantified by the "degree of trigonality" which is defined as $\tau = (\beta - \alpha)/60$, where '$\beta$' is the largest and '$\alpha$' the second largest of the L_{basal}–M–L_{basal} angles [10,11]. The limiting values are $\tau = 0$ for an ideal tetragonal geometry and $\tau = 1$ for an ideal trigonal-bipyramid. In the present case, we find $\beta = 167.66(9)°$ [N(1)–Ga–N(3)] and $\alpha = 127.18(10)°$ [N(2)–Ga(1)–N(4)] for **2** · 0.5MeOH · 0.5H_2O. Thus, a value of $\tau = 0.67$ is obtained for **2** · 0.5MeOH · 0.5H_2O. Hence the geometry around Ga(III) is best described as a distorted trigonal bipyramid (or a square-based pyramidal distorted trigonal bipyramid, SBPDTBP)

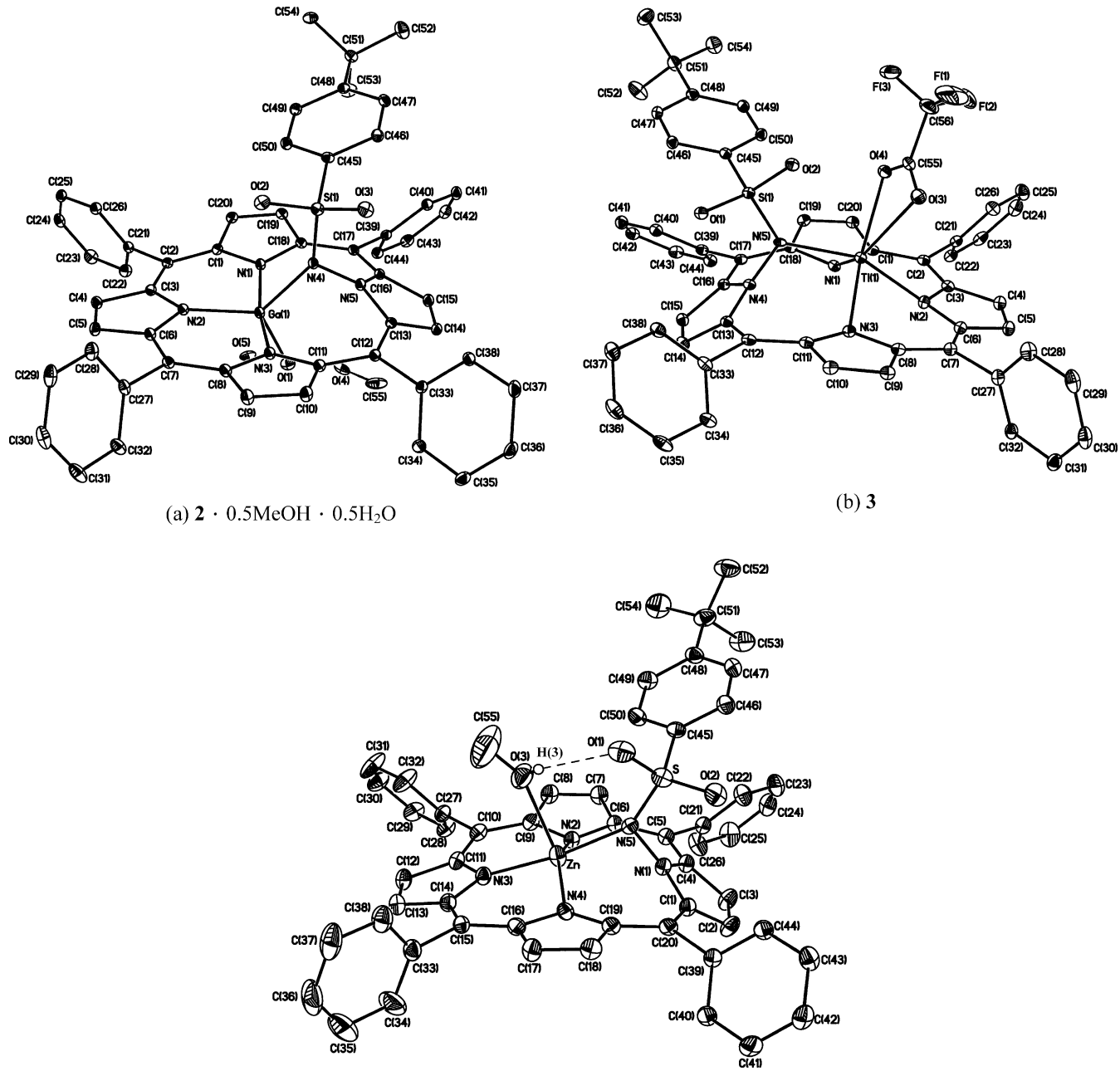

Fig. 1. Molecular configuration and atom-labeling scheme for (a) Ga(*N*-*p*-$NSO_2C_6H_4{}^tBu$tpp)(OH) · 0.5MeOH · 0.5H_2O [**2** · 0.5MeOH · 0.5H_2O], (b) Tl(*N*-*p*-$NSO_2C_6H_4{}^tBu$-tpp)(O_2CCF_3) **3** and (c) Zn(*N*-*p*-$NSO_2C_6H_4{}^tBu$-tpp) · 0.7MeOH [**4** · 0.7MeOH], with ellipsoids drawn at 30% probability. Hydrogen atoms for all compounds are omitted for clarity.

with N(2), N(4), and O(1) lying in the equatorial plane for **2** · 0.5MeOH · 0.5H_2O [12].

The pyrrole nitrogens N(5), N(4), and N(1) are no longer bonded to gallium, thallium, and zinc as indicated by their longer internuclear distances, 2.638(2) Å for Ga(1)···N(5), 2.880(2) Å for Tl(1)···N(4) and 2.627(6) Å for Zn···N(1). We adopt the plane of three strongly bound pyrrole nitrogen atoms [i.e., N(1), N(2), and N(3) for **2**, **3** and N(2), N(3), and N(4) for **4**] as a reference plane 3N. Because of the larger size of the Tl^{3+} in complex **3**, T^{3+} and N(5) are located on the same side at 1.14 and 1.41 Å from its (3N) plane, but for complex **2**, Ga^{3+} and N(4) are located on different sides at −0.17 and 1.27 Å from its (3N) plane, [cf. the corresponding displacement of 0.51 Å for Zn and 1.30 Å for N(5) in **4**]. Apparently, chelating bidentate trifluoroacetate in **3** is *cis* to the $NSO_2C_6H_4{}^tBu$ group with O(3) and O(4) being located separately at 3.17 and 3.01 Å out of the 3N plane and monodentate hydroxide in **2** is *trans* to the $NSO_2C_6H_4{}^tBu$ group with O(1) located at −1.86 Å out of the 3N plane.

Table 3
^{1}H,^{13}C NMR and X-ray data for complexes **2**, **3** and **4**

Compound	r_{ion} (Å)	X-ray		^{1}H NMR (ppm)			^{13}C NMR (ppm)
		Δ(3N)[a] (Å)	θ[b] (°)	^{t}BuBS-H$_{3,5}$	^{t}BuBS-H$_{2,6}$	^{t}Bu	ΔC_β[c]
Ga^{3+} in **2**	0.69	0.17	26.7	6.58	4.72	1.03	10–15
Zn^{2+} in **4**	0.74	0.51	39.6	6.89	5.58	1.15	15–17
Tl^{3+} in **3**	1.025	1.14	41.9	7.13	6.13	1.19	17–21

[a] Δ(3N) denotes the displacement of the metal center from the 3N plane.
[b] θ: dihedral angle between the pyrrole ring bearing a $NSO_2C_6H_4{}^tBu$ group and the 3N plane.
[c] $\Delta C_\beta = \delta C_\beta$ (bearing a $NSO_2C_6H_4{}^tBu$ group) − δC_β (without bearing a $NSO_2C_6H_4{}^tBu$ group).

The porphyrin macrocycle is indeed distorted because of the presence of the $NSO_2C_6H_4{}^tBu$ group. Thus, the N(5) (in **2**), N(4) (in **3**) and N(1) (in **4**) pyrrole rings bearing the $NSO_2C_6H_4{}^tBu$ group would be deviated mostly from the 3N plane and oriented separately in a dihedral angle of 26.7°, 41.9°, and of 39.6°, whereas small angles of 6.9°, 5.0°, and 8.6° occur with N(1), N(2), and N(3) pyrroles for **2** · 0.5MeOH · 0.5H_2O, and 11.6°, 7.9°, and 2.1° occur with N(1), N(2), and N(3) pyrroles for **3**, and 9.2°, 11.0° and 5.0° occur with N(2), N(3), and N(4) pyrroles for **4** · 0.7MeOH. In complex **2** · 0.5MeOH · 0.5H_2O, such a large deviation from planarity for the N(5) pyrrole is also reflected by observing a 10–15 ppm upfield shift of the C_β(C14,C15) at 120.1 ppm compared to 135.2 ppm for C_β(C10,C19), 133.2 ppm for C_β(C4,C5) and 129.7 ppm for C_β(C9,C20). In compound **3**, a similar deviation is found for the N(4) pyrrole by observing a 17–21 ppm upfield shift of the C_β(C14,C15) at 116.0 ppm compared to 136.8 for C_β(C10,C19), 134.0 ppm for C_β(C9,C20), and 132.6 ppm for C_β(C4,C5). In compound **4**, a similar deviation is also found for the N(1) pyrrole by observing a 15–17 ppm upfield shift of the C_β(C2,C3) at 117.6 ppm compared to 134.6 for C_β(C7,C18), 132.5 ppm for C_β(C12,C13) and 132.4 ppm for C_β(C8,C17). Similar kind of upfield shifts of C_β resonances due to the non-planarity of porphyrin were also observed with a magnitude of 15–17 ppm for Zn(N-NTs-tpp) and 16–21 ppm for Tl-(N-NTs-tpp)(OAc) [2,3]. In a nutshell, as the ionic radius increases from 0.69 Å for Ga^{3+}, 0.74 Å for Zn^{2+}, to 1.025 Å for Tl^{3+}, the bending of pyrrole ring bearing a $NSO_2C_6H_4{}^tBu$ group increases from **2**, **4** to **3**. Hence, the dihedral angles (θ) between the sharply bent pyrrole ring and the 3N plane increases from 26.7° in the gallium complex, 39.6° in the zinc complex, to 41.9° in the thallium complex (Table 3). Such a large bending from planarity is also reflected by observing the amount of the upfield shift for the C_β of the sharply bent pyrrole ring (i.e., ΔC_β). This ΔC_β increases from 10–15 ppm for **2**, 15–17 ppm for **4**, to 17–21 ppm for **3** (Table 3). The dihedral angles between the mean plane of the skeleton (3N) and the planes of the phenyl groups are 71.5° [C(24)], 69.6° [C(30)], 55.7° [C(36)], and 56.3° [C(42)] for **2** · 0.5MeOH · 0.5H_2O and 56.5° [C(24)], 83.5° [C(30)], 46.6° [C(36)], and 34.9° [C(42)] for **3** and the corresponding angles are 52.5°, 55.1°, 87.5°, and 47.2° for **4** · 0.7MeOH.

3.2. ^{1}H and ^{13}C NMR for (2) and (4) in $CDCl_3$ and (3) in CD_2Cl_2

Complexes **2**, **3** and **4** were characterized by ^{1}H (Fig. 2) and ^{13}C NMR spectra. In solution, the molecule has effective C_S symmetry with a mirror plane running through the N(2)–Ga(1)–N(4)–N(5) unit for **2** or the N(2)–Tl(1)–N(5)–N(4) unit for **3** or N(3)–Zn–N(5)–N(1) unit for **4**. There are four distinct β-pyrrole protons H_β, four β-pyrrole carbons C_β, four α-pyrrole carbons C_α, two different *meso* carbons C_{meso}, and two phenyl-C_1 carbons for all the three complexes. The NMR study of **3** showed four different types of Tl–H coupling constants for H_β in CD_2Cl_2 at 20 °C (Fig. 2b). The doublet at 8.81 ppm is assigned to H_β(4,5) with ^4J(Tl–H) = 90 Hz and the singlet at 7.03 ppm is due to H_β(14,15). The doublet of a doublet at 9.16 ppm is due to H_β(10,19) with ^4J(Tl–H) = 17.5 Hz and ^3J(H–H) = 4.8 Hz and the doublet of a doublet at 9.03 ppm is due to H_β(9,20) with ^4J(Tl–H) = 10.3 Hz and ^3J(H–H) = 4.8 Hz. Likewise, there were also four different types of Tl–^{13}C coupling constants for C_β in **3**. The doublet at 132.6 ppm is due to C_β(C4,C5) with ^3J(Tl–^{13}C) = 198 Hz and the doublet at 136.8 ppm is due to C_β(C10,C19) with ^3J(Tl–^{13}C) = 35 Hz. The singlet at 134.0 ppm is due to C_β(C9,C20) with ^3J(Tl–^{13}C) being unobserved and the doublet at 116.0 ppm is due to C_β(C14,C15) with ^4J(Tl–^{13}C) = 88 Hz. The ^{1}H NMR spectra reveal that the aromatic protons of the ^{t}BuBS group appear as two doublets at 6.58 (^{t}BuBS – $H_{3,5}$) and at 4.72 ppm (^{t}BuBS – $H_{2,6}$) for **2** (Fig. 2a) and at 7.13 (d) and 6.13 (d) ppm for **3** (Fig. 2b).

Due to the porphyrin ring current effect, all $NSO_2C_6H_4{}^tBu$ and hydroxo protons are shifted upfield compared to their counterparts in free $NSO_2C_6H_4{}^tBu$ and OH^-. The above ring current effect indicates that the $NSO_2C_6H_4{}^tBu$ group is bonded to Zn in **4** and to Tl in **3** and both the $NSO_2C_6H_4{}^tBu$ and the OH^- ligands are bonded to Ga in **2** in solution phase. The NSO_2-$C_6H_4{}^tBu$ bonding argument is further corroborated by the result that the ^{t}BuBS-C_1 [i.e., C(45)] in **3** was observed at 137.7 ppm with ^3J(Tl–C) = 52 Hz. X-ray diffraction analysis unambiguously confirms that **3** is a bidentate complex in the solid phase. Broadly, by increasing Δ(3N) from 0.17 Å for (Ga^{3+} in **2**), 0.51 Å for (Zn^{2+} in **4**) to 1.14 Å for (Tl^{3+} in **3**), the δ(^{t}BuBS-$H_{2,6}$)

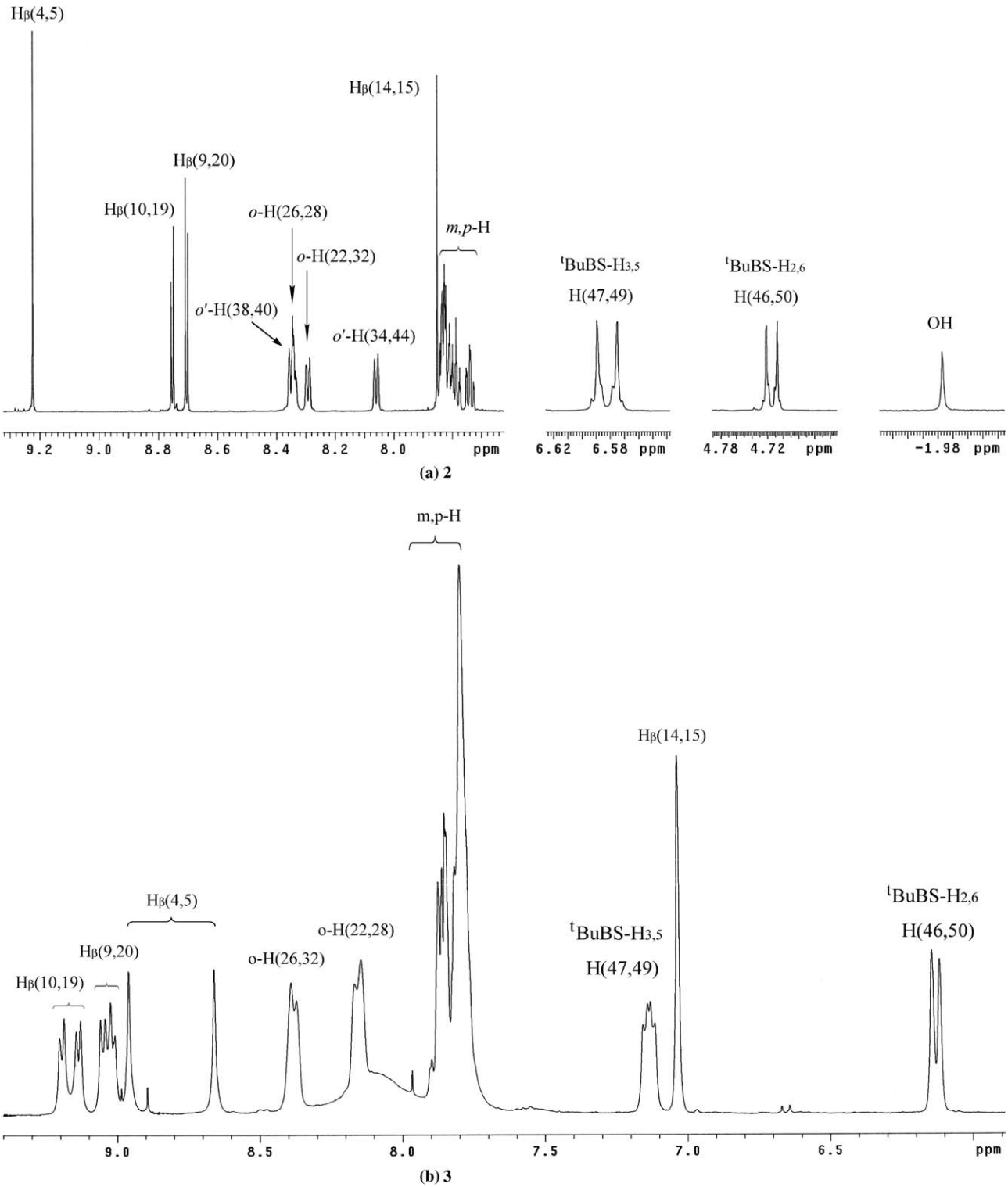

Fig. 2. ^{1}H NMR spectra for (a) **2** in $CDCl_3$ at 599.95 MHz and (b) **3** in CD_2Cl_2 at 299.96 MHz.

shifts from 4.72, 5.58 to 6.13 ppm and $\delta(^t\text{BuBS-H}_{3,5})$ shifts from 6.58, 6.89 to 7.13 ppm (Table 3). The ring current effect for the ^{1}H resonances of the ^{t}BuBS protons decreases with an increase in the distance between ^{t}BuBS protons and C_t. The geometrical center (C_t) is the center of the mean plane of the 4N atoms core [i.e., N(1), N(2), N(3) and N(5) for **2**, N(1)–N(4) for **3** and **4**]. The above results suggest that as the protons of the ^{t}BuBS are located on metal with a large Δ3N, they move away from the geometrical center C_t of 4N for the complexes **2**, **3** and **4**. Hence, the shielding of the ring current effect from the 18π electrons becomes smaller and the ^{1}H chemical shifts are relatively less upfield than those with a smaller Δ3N.

For *ortho* protons, at 20 °C, the rotation of phenyl group along C_1–C_{meso} bond for **2** in $CDCl_3$ is intermediately slow which is evident from the appearance of the two sets of doublet, one multiplet and one singlet due to four different *ortho* protons of aromatic ring (Fig. 2a) [13]. For these *ortho* protons in **2**, we attribute one multiplet at 8.34 ppm to *ortho* protons *o*-H(26,28), the doublet at 8.29 ppm to *ortho* protons *o*-H(22,32) with ^3J(H–H) = 5.4 Hz, one singlet at 8.36 ppm due to *ortho* protons *o′*-H(38,40) and the other doublet at 8.06 ppm is assigned to *ortho* protons *o′*-H(34,44) with ^3J(H–H) = 4.3 Hz (Fig. 2a). This rotation of the phenyl group along C_1–C_{meso} [C(7)–C(27) or C(2)–C(21)] bond for **3** in CD_2Cl_2 at 20 °C is also intermediately slow. This intermediately slow rotation is supported by the two doublets at 8.38 and 8.15 ppm due to *o*-H(26,32) and *o*-H(22,28), respectively. Moreover, the rotation of phenyl group along the C(12)–C(33) [or C(17)–C(39)] bond for **3** is at the intermediate exchange region. In this intermediate exchange region, the signals are broadened beyond detection. Hence, no signals of *o′*-H(34,44) and *o′*-H(38,40) for **3** have been observed at 20 °C (Fig. 2b).

3.3. Dynamic NMR of 3 in CD_2Cl_2

Upon cooling of a 0.02M CD_2Cl_2 solution of **3**, the ^{19}F signals of $CF_3CO_2^-$ being a single peak at 20 °C ($\delta = -73.50$ ppm), first broadened (coalescence temperature $T_c = -50$ °C) and then split into two peaks ($\delta = -72.92$ ppm) with a separation of 29.4 Hz at −90 °C. As the exchange of $CF_3CO_2^-$ within **3** is reversible, the results at 564.49 MHz confirm the separation as a coupling of ^4J(Tl–F) rather than a chemical shift difference.

3

$$\xrightleftharpoons{CD_2Cl_2} \text{Tl(N-}p\text{-NSO}_2\text{C}_6\text{H}_4{}^t\text{Bu-tpp)}^+ + CF_3CO_2^- \quad (1)$$

The loss of coupling is due to reversible dissociation of $CF_3CO_2^-$ with a small dissociation constant [14]. Such a scenario would lead to the change in the chemical shift with temperature and no detectable free $CF_3CO_2^-$ and Tl-(N-p-$NSO_2C_6H_4{}^tBu$-tpp)$^+$ at low temperature, but would lead to the loss of coupling between trifluoroacetate and thallium at higher temperature. The chemical shift in the high-temperature limit is the average of the two species [i.e., Tl(N-p-$NSO_2C_6H_4{}^tBu$-tpp)(O_2CCF_3) and $CF_3CO_2^-$] in Eq. (1) weighted by their concentration. The free energy of activation $\Delta G^{\ddagger}_{223} = 46.3$ kJ/mol is therefore determined for the intermolecular exchange of $CF_3CO_2^-$ in **3**.

At 20 °C, intermolecular exchange of the $CF_3CO_2^-$ group is rapid as indicated by the appearance of quartet signal due to carbonyl carbon [δ 160.7, ^2J(F–C) = 39 Hz] for **3** in CD_2Cl_2, but no Tl–^{13}C splitting was observed. Moreover, no signal of CF_3 carbons has been found for **3** in CD_2Cl_2 at 20 °C. At −90 °C, the rate of intermolecular exchange of $CF_3CO_2^-$ for **3** in CD_2Cl_2 is slow. Hence, at this temperature, the CO and CF_3 carbons of $CF_3CO_2^-$ in **3** are observed at δ 160.2 ppm [with ^2J(F–C) = 40 and ^2J(Tl–C) = 81 Hz] and 115.9 ppm [^1J(F–C) = 290 and ^3J(Tl–C) = 155 Hz], respectively. These ^{13}C resonances are quite close to that of trifluroacetato-*N*-tosylimido-*meso*-tetraphenylporphyrinatothallium(III) Tl(N-NTs-tpp)-(O_2CCF_3) **5** in which the two corresponding carbons were observed at δ 160.1 ppm [with ^2J(F–C) = 38.6 and ^2J(Tl–C) = 83 Hz] and 115.7 ppm [^1J(F–C) = 287.2 and ^3J(Tl–C) = 154 Hz] respectively in CD_2Cl_2 at −90 °C [15]. These ^{13}C resonances are also quite close to that of Tl(tpp)(O_2CCF_3) in which the two corresponding carbons were observed at 156.5 ppm [with ^2J(Tl–C) = 128 Hz, and ^2J(F–C) = 37 Hz] and 115.9 ppm [with ^3J(Tl–C) = 239 Hz and ^1J(F–C) = 291 Hz] in THF-d_8 at −100 °C but with different $^{2,3}J$(Tl–C) coupling constants [9]. An electronegative substituent, N(5), with a group electronegativity $\chi = 2.98$ bonded to Tl(l) in **3** and the torsion angle of $\Psi_{N-C_\gamma}(N\text{–}Tl_\alpha\text{–}O_\beta\text{–}C_\gamma) = -79.7°$ cause a significant negative contribution up to 84 Hz for Δ^3J(Tl–C, N) = [^3J(Tl–C, **3**) − ^3J(Tl–C, Tl(tpp)(O_2CCF_3))] = 155–239 and 47 Hz for Δ^2J(Tl–C, N) = [^2J(Tl–C, **3**) − ^2J(Tl–C, Tl(tpp)-(O_2CCF_3))] = 81–128 of $CF_3CO_2^-$ in **3** [16–21].

To conclude, we have investigated for the first time the three diamagnetic, mononuclear, and bridged metal complexes of 21-(4-*tert*-butyl-benzenesulfonamido)-5,10,15,20-tetraphenyl-porphyrin having M–N–(p-$SO_2C_6H_4{}^tBu$)–N [or M–N–^{t}BuBS–N, M = Ga(III), Tl(III), Zn(II)] linkage, and their X-ray structures are analyzed. The unambiguous assignments of ^1H NMR data for **2** and **4** in $CDCl_3$ and **3** in CD_2Cl_2 are reported in this work. Dynamic ^{19}F and ^{13}C NMR spectra of the trifluoroacetato group in **3** reveal that this group undergoes an intermolecular exchange with a free energy of activation, $\Delta G^{\ddagger}_{223} = 46.3$ kJ/mol. Thus, the tpp complexes were thoroughly studied and characterized both by dynamic NMR and X-ray crystallography. The correlation of Δ3N of the metal ion either with its ionic radius or with the ^1H ring current effect from the protons of ^{t}BuBS group for compounds **2**, **3** and **4** is clearly explained. Mean while, the correlation of the ionic radius of metal ion either with the dihedral angle (θ) between the bent pyrrole ring and the 3N plane or with ΔC_β [$=\delta C_\beta$ (bearing a $NSO_2C_6H_4{}^tBu$ group) − δC_β (without bearing a $NSO_2C_6H_4{}^tBu$ group)] is also depicted unambiguously.

4. Supplementary material

Crystallographic data in GIF format for **2**, **3** and **4** have been deposited with Cambridge Data Centre as CCDC No. 280262 (for **2** · 0.5MeOH · 0.5H_2O), CCDC No. 280263 (for **3**) and CCDC No. 280264 (for **4** · 0.7MeOH), respectively. The three solvent protons in **2** · 0.5MeOH · 0.5H_2O are not added in the file of CIF. Copies of this information

may be obtained free of charge from The Director, CCDC, 12 Union Road, Cambridge, CB2 1EZ, UK on request (fax: +44 1223 336033; e-mail deposit@ccdc.cam.ac.uk or www: http://www.ccdc.cam.ac.uk).

Acknowledgement

Financial support from the National Research Council of the R.O.C. under Grant NSC 93-2113-M-005-015 is gratefully acknowledged.

References

[1] H.J. Callot, B. Chevrier, R. Weiss, J. Am. Chem. Soc. 100 (1978) 4733.
[2] J.Y. Tung, J.I. Jang, C.C. Lin, J.H. Chen, L.P. Hwang, Inorg. Chem. 39 (2000) 1106.
[3] Y.I. Li, C.S. Chang, J.Y. Tung, C.H. Tsai, J.H. Chen, F.L. Liao, S.L. Wang, Polyhedron 19 (2000) 413.
[4] C.S. Chang, C.H. Chen, Y.I. Li, B.C. Liau, B.T. Ko, S. Elango, J.H. Chen, Inorg. Chem. 40 (2001) 2905.
[5] C.H. Chen, Y.Y. Lee, B.C. Liau, S. Elango, J.H. Chen, H.Y. Hsieh, F.L. Liao, S.L. Wang, L.P. Hwang, J. Chem. Soc., Dalton Trans. (2002) 3001.
[6] F.A. Yang, J.H. Chen, H.Y. Hsieh, S. Elango, L.P. Hwang, Inorg. Chem. 42 (2003) 4603.
[7] J.P. Mahy, P. Battioni, G. Bedi, D. Mansuy, J. Fishcher, R. Weiss, I. Morgenstern-Badarau, Inorg. Chem. 27 (1988) 353.
[8] J.E. Huheey, E.A. Keiter, R.L. Keiter, Inorganic Chemistry, 4th ed., Harper Collins College Publishers, New York, 1993, p. 114, 292.
[9] L.F. Chou, J.H. Chen, J. Chem. Soc., Dalton Trans. (1996) 3787.
[10] A.W. Addison, T.N. Rao, J. Reedijk, J.V. Rijn, G.C. Verchoor, J. Chem. Soc., Dalton Trans. (1984) 1349.
[11] R.G. Garvey, R.O. Koob, M.L. Morris, Acta Crystallogr., Sect. C 43 (1987) 2056.
[12] G. Murphy, P. Nogle, B. Murphy, B. Hathaway, J. Chem. Soc., Dalton Trans. (1997) 2645.
[13] R.S. Drago, Physical Methods for Chemists, 2nd ed., Saunder College Publishing, New York, 1992, p. 291.
[14] J.P. Jensen, E.L. Muetterties, in: L.M. Jackman, F.A. Cotton (Eds.), Dynamic Nuclear Magnetic Resonance Spectroscopy, Academic Press, New York, 1975, p. 299.
[15] S.W. Chiou, J.H. Chen, personal communication.
[16] H. Liu, Q. Wang, L. Liu, J. Chem. Educ. 69 (1992) 783.
[17] J.A. Schwarcz, N. Cyr, A.S. Perlin, Can. J. Chem. 53 (1975) 1872.
[18] R.H. Contreras, J.E. Peralta, Prog. Nucl. Magn. Reson. 37 (2000) 321.
[19] M. Morvai, T. Nagy, A. Kocsis, L.F. Szabo, B. Podanyi, Magn. Reson. Chem. 98 (2000) 343.
[20] J.S. Fabian, J. Guilleme, E. Diez, J. Mol. Struct. (Theochem.) 426 (1998) 117.
[21] F.A. Yang, K.Y. Cho, J.H. Chen, S.S. Wang, J.Y. Tung, H.Y. Hsieh, F.L. Liao, S.L. Wang, L.P. Hwang, S. Elango, personal communication.